

Fort Hays State University

FHSU Scholars Repository

Master's Theses

Fall 2018

Osteohistology And Skeletochronology Of An Ontogenetic Series Of Clidastes (Squamata: Mosasauridae): Growth And Metabolism In Basal Mosasaurids

Cyrus C. Green

Fort Hays State University, ccgreen@mail.fhsu.edu

Follow this and additional works at: <https://scholars.fhsu.edu/theses>



Part of the [Geology Commons](#), [Paleobiology Commons](#), and the [Paleontology Commons](#)

Recommended Citation

Green, Cyrus C., "Osteohistology And Skeletochronology Of An Ontogenetic Series Of Clidastes (Squamata: Mosasauridae): Growth And Metabolism In Basal Mosasaurids" (2018). *Master's Theses*. 3123.

DOI: 10.58809/MQVC1909

Available at: <https://scholars.fhsu.edu/theses/3123>

This Thesis is brought to you for free and open access by FHSU Scholars Repository. It has been accepted for inclusion in Master's Theses by an authorized administrator of FHSU Scholars Repository. For more information, please contact ScholarsRepository@fhsu.edu.

OSTEOHISTOLOGY AND SKELETOCHRONOLOGY OF AN ONTOGENETIC
SERIES OF *CLIDASTES* (SQUAMATA: MOSASAURIDAE): GROWTH
AND METABOLISM IN BASAL MOSASAURIDS

being

A Thesis Presented to the Graduate Faculty
of the Fort Hays State University in
Partial Fulfillment of the Requirements for
the Degree of Master of Science

by

Cyrus C. Green

B.A., University of Colorado, Denver

Date _____

Approved _____
Major Professor

Approved _____
Chair, Graduate School

ABSTRACT

Clidastes was a large marine reptile from the Late Cretaceous Western Interior Seaway of North America. Though the remains of *Clidastes* have been found in the Cretaceous chinks and shales for over 150 years, little is known about their growth rates. Osteohistology is a well-documented technique used to investigate growth in extinct animals. Previous histological studies of *Clidastes* have hypothesized higher growth rates in basal mosasaurids than varanids due to higher vascularity. These studies focused on adult specimens but did not look at ontogenetic changes in growth rates. Isotopic studies of *Clidastes* indicate high metabolic temperatures, leading to speculation these animals had either gigantothermic or endothermic metabolisms. Whether the growth rates in *Clidastes* are comparable to endothermic or ectothermic animals has not been studied. This study uses osteohistology and skeletochronology to determine age at the time of death, investigate ontogenetic changes in internal bone microstructure, and estimate growth rates through *Clidastes* ontogeny.

Four humeri representing a size gradient in *Clidastes* were histologically analyzed. Skeletochronological ages of the four specimens are yearling (<1 year), juvenile (3-4 years), sub-adult (6-7 years), and possible adult (13-14 years). All humeri show parallel-fibered bone as the main tissue type. Vascularity and growth rates decrease as size and age increase through *Clidastes* ontogeny. Primary osteons and radial canals seen in early ontogeny decrease until only longitudinal simple canals remain in late ontogeny. Though no growth marks are visible in the yearling, vascularity is much higher than the other specimens, suggesting a higher growth rate during the first year of life. In the juvenile, growth rates in the second year of life are $1.70 \mu\text{m}(\text{day})^{-1}$. In the sub-adult,

growth rates in years four and five are 1.65 and 1.75 $\mu\text{m}(\text{day})^{-1}$ respectively. In the largest humerus, growth rates in years eight through eleven are variable, but all are less than 0.80 $\mu\text{m}(\text{day})^{-1}$. No humeri show evidence of skeletal maturity, though the slowing of growth in the largest humerus could represent sexual maturity or the onset of skeletal maturity.

Clidastes grew fastest during the first year of life. Growth slowed during the second year but continued at this same rate until after the sixth or seventh year when it slowed again. While this study finds that vascularity in *Clidastes* is greater than modern varanids, growth rates are more comparable to ectothermic than endothermic animals. Growth rates determined in this study support the gigantothermic rather than endothermic metabolic hypothesis for *Clidastes*.

ACKNOWLEDGEMENTS

I would like to thank my thesis committee, Dr. Laura Wilson, Dr. Reese Barrick, and Dr. Jonathan Sumrall who gave advice and comments on drafts of this work. Special thanks to my advisor, Dr. Wilson, who questioned me and guided me through this project, always trying to steer me in the right direction, even though I sometimes did not listen. Your constant push made me a better scientist and writer.

I would like to thank my father, Richard Green, without whose constant words of encouragement and acclamation this work would not have been possible. Thank you to my Uncle Stu and Aunt Terri who provided me with many sushi dinners and much needed drinks.

Thank you to Jun Ebersol at the Mcwane Science Center and Dana Ehret at the University of Alabama, Birmingham for allowing me to visit and scrounge through your collections, and for allowing me to borrow the humeri used for this study.

Many thanks to the following people for giving me advice, listening to me complain, buying me drinks, and making me laugh; I couldn't have done it without any of you: Molly and Thomas d'Aquin, Silas and Gavin d'Aquin, Suzanne Magnuson, Curt Wallach, Olivia Quintana, Corine Roberts-Niemann, Dyin' Joe Burkins, Mathew Lilly, Anna Castano, The Goddard Family, Jessica Barnett, Pike Holman, Megan Osborn, Patrick Wilson, Tom Buskuskie, Jenny Feeney, Christina Byrd, Amber Michels, Logan King, Teresa Bauer, Hillary Mclean, Josh Lively, The Durham Family, Alexandra Houssaye, Hallie Street, JP and Becky Cavigelli, Dewayne Wagoner, Melissa Conelly, Michelle Mekarski, Rachel Unruh (thanks for the lasagna!!!), Kent Issacson, Beverly Cousins, Rebecca Barnett, Patti Finkle, Chase Shelburne, Ian Trevethan, Dean Zerr, JP

Finkle (Dr. Awkward rules!), Melissa Macias, Helen and Rex Hoff, Darrah Steffen, Meena Madan, Bruce Rothschild, Kelsie Abrams, Russell Hawley, Curtis Schmidt, Patricia Duffy, Melissa Glenn, Rick Buck, Lilly and Shawn Mclellan, Steven Pfaff, Kat Rivers, Hannah Horinek, Shayne O'Brien, Anthony Maltese, Elizabeth Schumann, Trever Williams, Kaitlyn Gauvey, Cody Gibson, Kris Super, Hank Woolley, Mitch Sommers.

TABLE OF CONTENTS

	Page
ABSTRACT.....	i
ACKNOWLEDGEMENTS.....	iii
TABLE OF CONTENTS.....	v
LIST OF TABLES.....	vi
LIST OF FIGURES.....	vii
INTRODUCTION.....	1
MATERIALS and METHODS.....	7
RESULTS.....	12
DISCUSSION.....	28
CONCLUSION.....	36
LITERATURE CITED.....	38

LIST OF TABLES

Table	Page
Table 1: Size of humeris studied.....	8
Table 2: Longitudinal vascularity	12
Table 3: Distances between CGMs.....	17
Table 4: Retrocalculations of missing CGMs.....	23
Table 5: Growth rates.....	26

LIST OF FIGURES

Figures	Page
Figure 1: Humeri used for this project.....	8
Figure 2: Example of how radii measurements were taken.....	11
Figure 3: Transverse cross section of RMM 6066.....	13
Figure 4: Cortical area of RMM 6066.....	14
Figure 5: Cortical area of RMM 6066.....	14
Figure 6: Transverse cross section of ALMNH 5186.....	16
Figure 7: Trabeculae of ALMNH 5186.....	16
Figure 8: Cortical bone of ALMNH 5186.....	18
Figure 9: Cortical area of ALMNH 5186.....	18
Figure 10: Cortical bone of ALMNH 5186 with pathology.....	20
Figure 11: Cortical area of ALMNH 5186 in longitudinal cut.....	20
Figure 12: Transverse cross section of ALMNH 4332.....	22
Figure 13: Trabeculae of ALMNH 4332.....	22
Figure 14: Cortical area of ALMNH 4332 in longitudinal cut.....	24
Figure 15: Cortical area of ALMNH 4332.....	24
Figure 16: Transverse cross section of RMM 2986.....	25
Figure 17: Trabeculae of RMM 2986.....	27
Figure 18: Cortical bone of RMM 2986.....	27

INTRODUCTION

Clidastes (Mosasaurinae) was a predatory marine reptile that inhabited both open ocean and inland sea habitats during the Late Cretaceous (100-65 mya). Compared to other Mosasaurinae genera (i.e. *Prognathodon* and *Mosasaurus*), *Clidastes* was small with average lengths ranging from three to four meters, though larger specimens are known (Bell, 1997). As a secondarily aquatic animal, *Clidastes* evolved morphological specializations and adaptations that aided an aquatic lifestyle. These changes include reduction of the sacrum (Caldwell, 2002), hyperphalangy and flattening and elongation of the limb bones (Lindgren et al., 2011), an addition of caudal vertebrae to aid in locomotion (Lindgren et al., 2011), a switch from oviparity to viviparity (Caldwell and Lee, 2001; Field et al., 2015), and changes in bone microstructure (Sheldon, 1997; Houssaye, 2009; Houssaye and Bardet, 2012).

The purpose of this study is to use osteohistology and skeletochronology to analyze the bone microstructure of *Clidastes* humeri by 1) comparing ontogenetic changes in *Clidastes* medullary compactness, bone tissue type, and the quantity and direction of vascular canals, and by 2) using cyclical growth marks (CGMs) to retrocalculate age at time of death and estimate growth rates represented in cortical sections. Additionally, comparing *Clidastes* growth rates to known ectothermic and endothermic growth rates can aid in understanding mosasaur metabolism.

Osteohistology is a well-documented technique used to investigate phylogeny, mechanics, environment, and ontogenetic growth in extinct animals. Rather than an open medullary cavity, mosasaurids display a medullary area filled with a trabecular network, which is thought to aid in buoyancy and body trim controls (Sheldon, 1997; Houssaye,

2009; Houssaye and Bardet, 2012). Previous studies have shown a discrepancy in the ontogenetic changes in medullary compactness among different *Clidastes* bones.

Houssaye and Bardet (2012) show juvenile and adult *Clidastes* have similar vertebral medullary compactness, but Bell and Sheldon (1986) show juvenile *Clidastes* ribs have open medullary areas while adult ribs are compact. How this medullary area forms and why there are differences between juvenile vertebrae and rib medullary compactness has yet to be explored.

The correlation between growth rates and bone microstructure was first examined by Amprino (1947), who predicted that primary bone tissue type corresponded to different growth rates in an individual. Later studies confirmed these results, finding that differences in tissue type reflect growth rates with lamellar and parallel-fibered bone growing slower than woven bone (Castanet et al., 2000; de Margerie et al., 2004). Differences in vascular density and vascular orientation also reflect varying growth rates. Bones with a high vascular density grow faster than those with lower vascular density (de Ricqlès, 1976; de Buffrenil et al., 2008) and bone containing longitudinal canals generally grow at a slower rate than bone containing reticular and radial canals (de Ricqlès, 1976; Castanet et al., 2000; de Margerie et al., 2002). Osteohistology can also be used to determine if bone contains an external fundamental system (EFS) which denotes an animal has reached skeletal maturity. The EFS is found along the periosteal surface, typically in long bones, and is usually nonvascular and comprised of slow growing tissues with well-organized collagen fibers (Cormack, 1987; Starck and Chinsamy, 2002; Ponton et al., 2004; Woodward et al., 2011). EFSs have been found in a variety of animals including dinosaurs (Erickson et al., 2004; Horner and Padian, 2004; Padian et

al., 2004), alligators (Woodward et al., 2011), and monitor lizards (de Buffrenil and Castanet, 2000). An EFS has yet to be reported in mosasaurids.

Previous osteohistological studies of mosasaurids have used bone tissue type and vascularity in vertebrae, ribs, and limb bones to infer growth rates (Pellegrini, 2007; Houssaye, 2008; Houssaye and Bardet, 2012; Houssaye and Tafforeau, 2012; Houssaye et al., 2013). Parallel-fibered bone is the dominant bone tissue type across mosasaurid phylogeny (Houssaye et al., 2013). Woven fibered tissue has been found in small sections of cortical bone, with lamellar bone concentrated around the primary and secondary osteons and along the edges of trabeculae (Houssaye and Bardet, 2012; Houssaye et al., 2013). Houssaye et al., (2013) also found what they called unusual parallel-fibered bone (UPFB) and described it as bone that is anisotropic under polarized light (a property of parallel-fibered and lamellar bone tissue) but contains large, rounded osteocyte lacunae (a property of woven bone tissue). Radial and longitudinal primary osteons and simple canals are also common throughout mosasaurid phylogeny and ontogeny (Houssaye and Bardet, 2012; Houssaye and Tafforeau, 2012; Houssaye et al., 2013). By focusing on vascular canal density and orientation, studies hypothesize that mosasaurids grew slightly faster than modern monitor lizards but still relied on protracted, rather than rapid, growth in order to reach large size (Houssaye and Bardet, 2012). Consequently, growth rates in *Clidastes* are described as being somewhere above the extant turtle *Dermochelys* but lower than what has been suggested for extinct ichthyosaurs (Houssaye et al., 2013). However, the previous histological studies of mosasaurids have primarily focused on phylogenetic differences rather than ontogenetic differences. Sampling the same bone of individuals of different sizes in one taxon can give a comprehensive history of bone

growth through ontogeny (Chinsamy, 1995; Curry, 1999; Horner et al., 2000). A few histological studies of mosasaurids have sectioned smaller *Clidastes* vertebrae (Houssaye and Tafforeau, 2012) and limb bones (Pellegrini, 2007; Houssaye et al., 2013) that were considered juveniles and compared them with larger *Clidastes* vertebrae and limb bones that were considered adults, but a more comprehensive ontogenetic series of the genus has not been completed to date.

Skeletochronology is a well-established technique used to obtain an estimate of age in an extinct animal at the time of death (Castanet and Smirina, 1990; Chinsamy, 1993, 1995; de Buffrenil and Castanet, 2000; Horner et al., 2000; Horner and Padian, 2004; Woodward et al., 2013) and measure daily or yearly growth rates of an individual (Padian et al., 2001; Sander and Tückmantel, 2003; Montes et al., 2007; Cubo et al., 2008; Padian and Stein, 2013). Skeletochronological methods are based on counting CGMs. Studies have shown that when bone growth is interrupted due to seasonal cues or slowed due to natural biological rhythms, a ring representing arrested growth can occur in both ectothermic animals (e.g., de Ricqlès, 1976; Castanet and Smirina, 1990; Castanet, 1994; de Buffrenil and Castanet, 2000; de Buffrenil et al., 2008; Woodward et al., 2014) and endothermic animals (e.g., de Buffrenil et al., 1990; Sander and Andrassy, 2006; Köhler et al., 2012; Houssaye et al., 2015). Age estimation through retrocalculation has been accomplished by using the width of smaller sized (assumed younger) bones as proxy for bone resorbed in adults (Chinsamy, 1993, 1995) and by using the distances between preserved CGMs to calculate how much bone has been resorbed (Erickson, 2000; Horner et al., 2000; Horner and Padian, 2004).

The metabolism of mosasaurids has been studied previously, but studies do not agree whether the animals had ectothermic or endothermic metabolisms. Bernard et al (2010) conducted isotopic studies on mosasaurid teeth and concluded that mosasaurids in general had body temperatures higher than ambient sea temperatures. These high body temperatures were thought to stem from a gigantothermic metabolism. This type of metabolism—involving a large body having more surface area to volume ratio—is found in the modern leatherback turtle *Dermochelys* (Paladino et al., 1990). Recently, isotopic analysis of $\delta\text{O}^{18}_{\text{PO}_4}$ in enamel and bone from *Clidastes* of the Mooreville chalk showed that *Clidastes* body temperatures ranged from 30.0°C to ~37.0°C (Harrell et al., 2016), which is also higher than the average water temperature reconstructions of the Mooreville chalk (Liu, 2009). However, rather than a gigantothermic metabolism, Harrell et al. (2016) concluded *Clidastes* was endothermic.

Studies have shown that growth rates are closely correlated to metabolism. Endothermic animals tend to have high growth rates of 15 $\mu\text{m}(\text{day})^{-1}$ or above (Padian et al., 2001; de Margerie et al., 2004; Chinsamy and Hurum, 2006). Growth rates among ectothermic animals range from 0-10 $\mu\text{m}(\text{day})^{-1}$ (Padian et al., 2001; Montes et al., 2007; Cubo et al., 2008). Though exactly from where Mosasauridae derived is still in contention (see Lee, 1997; Conrad et al.; 2008) mosasaurids are considered squamates, and all modern squamates have ectothermic metabolisms (King and Green, 1999). The growth rate of extant squamates is usually on the lower end, growing at 0-2 $\mu\text{m}(\text{day})^{-1}$ (Montes et al., 2007; Cubo et al., 2008), though some neonate varanids can have growth rates of 7-9 $\mu\text{m}(\text{day})^{-1}$ (Cubo et al., 2012). Growth rates can then be used to discern a metabolic rate in *Clidastes*. Growth rates in *Clidastes* have only been reported with

qualitative assessments of vascularity and bone tissue type (Pellegrini, 2007; Houssaye and Bardet, 2012; Houssaye and Tafforeau, 2012; Houssaye et al., 2013) and not been reported quantitatively in microns per day. If Harrell et al. (2016) are correct in their conclusion of an endothermic metabolism for *Clidastes*, then growth rates measured quantitatively should have the high growth rates found in endothermic animals rather than slower growth rates found in ectothermic animals.

MATERIALS and METHODS

Four *Clidastes* humeri were selected for osteohistological analysis (Figure 1, Table 1). The four humeri were recovered from the *Clidastes* Acme-zone in the upper part of the Mooreville Chalk Formation of Alabama (Kiernan, 2002) and identified as *Clidastes* sp. The humeri belonged to four different individuals and were tentatively labeled as a neonate (RMM 6066), juvenile (ALMNH 5186), subadult (ALMNH 4332), and adult (RMM 2986) based on element size. RMM 6066 and RMM 2986 are from the McWane Science Center in Birmingham, AL, which houses the collections for the former Red Mountain Museum (RMM). ALMNH 5186 and ALMNH 4332 are from the Alabama Museum of Natural History (ALMNH) at the University of Alabama, Birmingham.

The humeri were measured with an electronic caliper (Table 1), sketched, photographed, and molded and cast prior to sectioning. Preparation for histological sampling followed Lamm (2013). A diaphyseal section was removed between the deltopectoral crest and the ectepicondyle process of each bone and embedded in Silmar 41 Clear Polyester Plastic Resin. The resin was placed in a vacuum to reduce bubbling and left to cure at room temperature for twenty-four hours. Thin sections were cut transversely from the proximal and distal ends of the resin-encased diaphyseal sections. In two bones, RMM 5186 and RMM 4332, thin sections were also cut longitudinally from the remaining diaphyseal section. These thin sections were adhered to slides using Devcon 2-Ton Epoxy and allowed to set for twelve hours. The adhered thin sections were ground using sandpaper and polished with a buffing cloth with 5 μ m aluminum powder. Slides were analyzed and photographed with an AmScope 300 Series microscope and

Table 1

Sizes of the four humeri studied. All measurements in cm. Lengths were taken from the most proximal to most distal end. Widths were taken from most anterior to posterior end. Diameter was taken at midshaft between the ectepicondyle and entepicondyle where cuts were made.

Specimen #	Length	Width	Circumference at mid-shaft
RMM 6066	2.0	1.4	3.1
ALMNH 5186	4.2	3.0	6.2
ALMNH 4332	7.3	5.9	9.2
RMM 2986	9.1	7.7	13.1



Figure 1: Humeri used for this project. A) RMM 6066, B) ALMNH 5186, C) ALMNH 4332, D) RMM 2986

AmScope 10-megapixel camera with Touptview© software. Photographs of the thin sections were edited using MosaicJ (an extension of ImageJ) software to stitch together complete cross sections of each bone.

To measure distances between CGMs and to account for CGMs lost to remodeling, other studies rely on the roundness of limb bones where radii are measured from the center to the corresponding CGM and averages taken

to account for medullary drift (Erickson, 2000; Sander and Tückmantel, 2003; Horner and Padian, 2004). This method of measurement was difficult for this study because mosasaurid appendicular bones are flattened and the radius in the anteroposterior direction is much longer than the radius in the dorsoventral direction. This study adopted

methods from Pellegrini (2007) who used Radius A as half the distance of the bone thickness in the anteroposterior direction and Radius B as half the distance in dorsoventral direction (Figure 2). However, due to heavy remodeling in the anteroposterior direction, CGMs are only visible in the dorsoventral direction of the humeri studied here, so only Radius B was used in calculations. CGMs were numbered with the CGM closest to the endosteal surface as CGM #1 and increased sequentially towards the periosteal surface. Distances between the CGMs were measured centrifugally (from the center outwards) along Radius B. To estimate the CGMs lost to remodeling, this study used methods similar to those used in Horner and Padian (2004). In that study, the cortical area is subtracted from the radius, leaving the medullary radius (MR). The radius of a smaller bone was then subtracted from the MR, leaving the resorbed cortical area (RCA) which was then divided by known CGM distances to estimate the number of resorbed CGM. In Horner and Padian (2004), the cortical and medullary areas of *Tyrannosaurus rex* are distinct, but in *Clidastes* humeri the medullary area is filled with trabeculae, making the distinction between these areas subtle, and making defining the cortical area difficult. One possibility was defining the cortical area as any area of bone near the periosteal surface not containing trabeculae. However, this would cause a loss of CGM as some CGM are found among newly formed trabeculae. A different option was defining the cortical area as the distance between CGM #1 and the periosteal surface. This option accounted for all CGM but meant trabeculae were included in the cortical area in some humeri and sections of cortical area were included in the medullary area in other humeri. Since the point of defining the cortical area is to aid in calculating how many CGM have been resorbed, defining the cortical area in this manner gives a more

accurate account of resorbed cortical area. Once the cortical area was defined in each bone, the methods followed Horner and Padian (2004). To date, RMM 6066 is the smallest humerus sectioned that has been described, so it is the reference point for deriving missing cortical area. Subtracting the Radius B of RMM 6066 from the calculated MR of a given bone leaves the RCA, which is the amount of cortical bone resorbed since the animal was the size and age of RMM 6066. To find the number of CGMs missing due to resorption, the RCA is divided by different distances previously measured: (i) maximum (largest CGM distance of that bone), (ii) penultimate (second largest CGM distance of that bone), and (iii) mean (average of all CGM distances of that bone) distances between CGMs, as previously described in Horner and Padian (2004) (See Table 3 for CGM distances). Because the distance between CGMs decreases as an animal ages, using the mean distance of CGMs from an ontogenetically older bone does not account for larger distances formed during early ontogeny already lost to remodeling. To solve this problem, a fourth measurement, (iv), was added using the mean of CGM distance (iii) of the most previous ontogenetically younger bone (see Table 4 for more on retrocalculations). The calculations made from these four categories gave a range for missing CGMs. The minimum and maximum numbers of missing CGMs obtained through all retrocalculations were averaged to get a better estimate of missing CGMs (Table 4).

To determine vascularity, a 10% section of the cortical area was measured in square centimeters (cm²) using ImageJ software. These sections consisted of the cortical area directly posterior of Radius B between the periosteal and endosteal surfaces (Figure 2). This 10% area represents the average vascularity at that time in ontogeny, preserved

in the bone at the time of death. Longitudinal vascular canals in each measured cortical area were counted using a microscope at 10x power. Dividing the counted canals by the measured area gives the longitudinal vascularity in canals $(\text{cm}^2)^{-1}$ (Table 2).

Distances between CGMs were divided by the number of days per year to get estimated $\mu\text{m}(\text{day})^{-1}$ of growth. Because the number of days per year has been getting progressively shorter since the Cambrian Period (Wells, 1969), calculations from Lee et al., (2013) were used to ascertain the days of the year during Late Santonian/Early Campanian (~80 mya) when the Mooreville Chalk was laid down (Kiernan, 2002). During this part of the Late Cretaceous there were ~372 days per year.

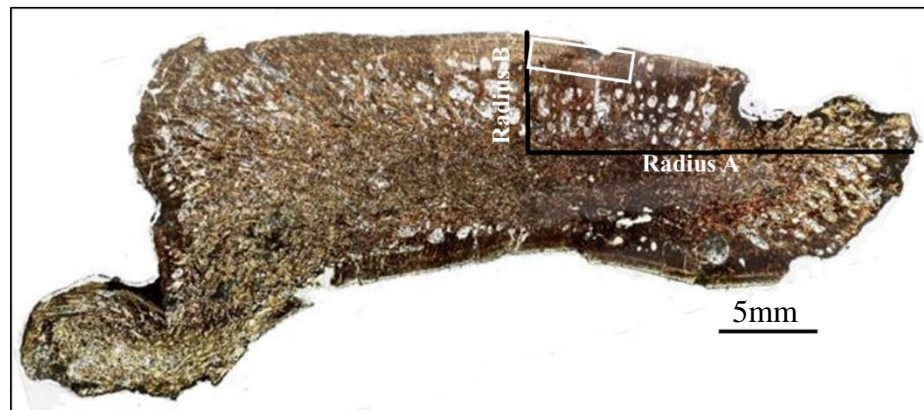


Figure 2: Example of how radii measurements were taken. All radial measurements were taken on transverse cuts through the diaphysis, as seen here in ALMNH 4332. Radius A is in the posterior direction and Radius B is in the dorsal direction. White square represents 10% of cortical area used to measure vascularity.

RESULTS

The humeri in this study display bone microstructure typical of mosasaurids (Pellegrini, 2007; Houssaye and Tafforeau, 2012; Houssaye et al., 2013), consisting of a network of trabeculae in the medullary area surrounded by a thin layer of cortical bone. Vascular architecture and orientation is consistent with previous studies (Houssaye and Bardet, 2012; Houssaye and Tafforeau, 2012; Houssaye et al., 2013). Vascular canals are a mix of simple canals and primary osteons arranged mostly longitudinally with few radial and reticular canals present. CGMs are found throughout the dorsal and ventral regions of the cortical bone in the humeri of this study. The anterior and posterior portions do not typically preserve records of growth cessation due to remodeling of those areas during ectepicondylar and entepicondylar processes growth. This observation is consistent with other studies of mosasaurid long bones (Pellegrini, 2007). As noted by Houssaye et al. (2013), expansion of the trabecular spaces usually begins with vascular canals found between CGMs. Some CGMs can still be seen where the medullary area meets the cortical bone and construction of trabeculae has begun. As expansion of the medullary area continues, these CGMs and all previous ontogenetic information are lost to resorption or construction of the trabeculae.

Table 2

Number of longitudinal canals found in 10% of cortical area posterior to the midline of the shaft.

Specimen #	# of Longitudinal Canals	Area of cortical bone examined (cm ²)	Longitudinal Vascularity canals(cm ²) ⁻¹
RMM 6066	62	3.058	20.27
ALMNH 5186	47	4.533	10.37
ALMNH 4332	80	7.683	10.41
RMM 2986	29	22.807	1.27

RMM 6066

The medullary area of RMM 6066 (Figure 3) is open with few large trabeculae crossing through the medullary area. The trabeculae and cortical bone surrounding the medullary area both appear anisotropic, indicating parallel-fibered bone (Figure 4). The collagen fibers show some organization but are not laid in concentric, alternating layers that would indicate lamellar bone. The trabeculae do not contain any lamellar bone along their edges. Both cortical bone and trabeculae contain osteocyte lacunae that are small and oblong. The cortical bone contains three distinct rows of longitudinally oriented primary osteons and simple canals (Figure 5). Simple radial and reticular canals connect some of the longitudinally oriented canals. Vascular canals also open to the periosteal surface. Longitudinal vascularity is $20.27 \text{ canals}(\text{cm}^2)^{-1}$ for this specimen (Table 2). There are no CGM observed in RMM 6066. It is not likely that any CGMs have been lost to resorption because there is little evidence of resorption or construction of the trabecular system.

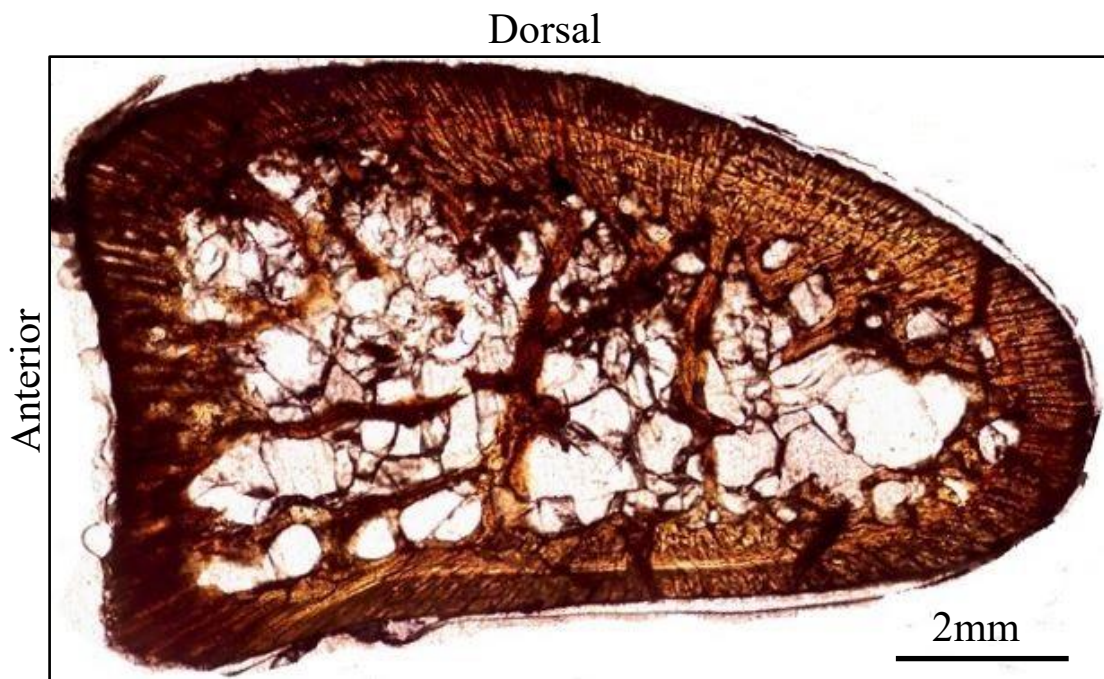


Figure 3: Transverse cross section of RMM 6066

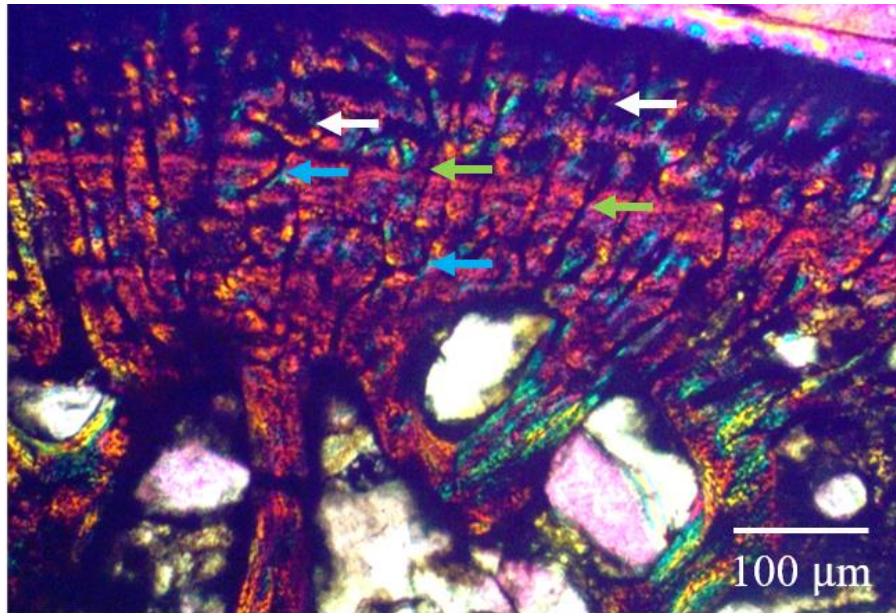


Figure 4: Cortical area of RMM 6066 under polarized light with longitudinal canals (white arrows), radial canals (green arrows), and reticular canals (blue arrows).

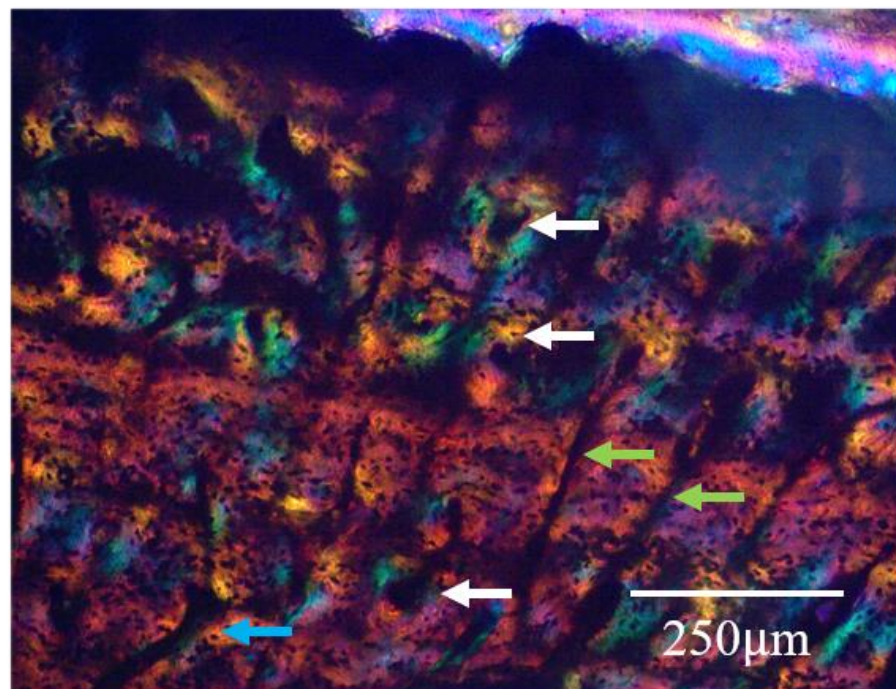


Figure 5: Cortical area of RMM 6066 under polarized light with longitudinal canals (white arrows), radial canals (green arrows), and reticular canals (blue arrows).

ALMNH 5186

The medullary area of ALMH 5186 is partially open, though trabeculae are more numerous than RMM 6066 (Figure 6). The trabeculae consist of parallel-fibered bone and areas of lamellar bone along the edges of trabeculae (Figure 7). The cortical bone consists of two distinct sections (Figures 8, 9, 10).

The cortical bone near the endosteum in ALMNH 5186 appears isotropic under polarized light, which typically indicates woven collagen fibers (Figure 9). However, isotropy occurs only in transverse view; when viewed longitudinally this bone appears anisotropic and is made of closely packed collagen fibers laid in parallel (Figure 11). Though unreported in mosasaurids, this longitudinally occurring parallel-fibered bone has been found in dinosaurs, and is thought to occur because the fibers line up longitudinally rather than transversely, giving the transverse cut the appearance of woven tissue (Stein and Prondvai, 2014). Osteocyte lacunae are small and oval shaped in both the trabeculae and the cortical area near the endosteum (Figures 9, 10). The longitudinal vascularity for ALMNH 5186 is $10.37 \text{ canals}(\text{cm}^2)^{-1}$ (Table 2). Two rows of longitudinally-oriented primary osteons and simple canals are situated between periods of arrested growth (Figures 8, 9). These canals are a mix of primary osteons and simple canals, are lined in neat rows, and are close together. The row of primary osteons closest to the endosteal surface has been almost completely resorbed due to formation of trabeculae.

The bone nearest the periosteum is parallel-fibered but is unlike any bone seen in other *Clidastes* specimens. It is likely that this bone is pathological in origin. A

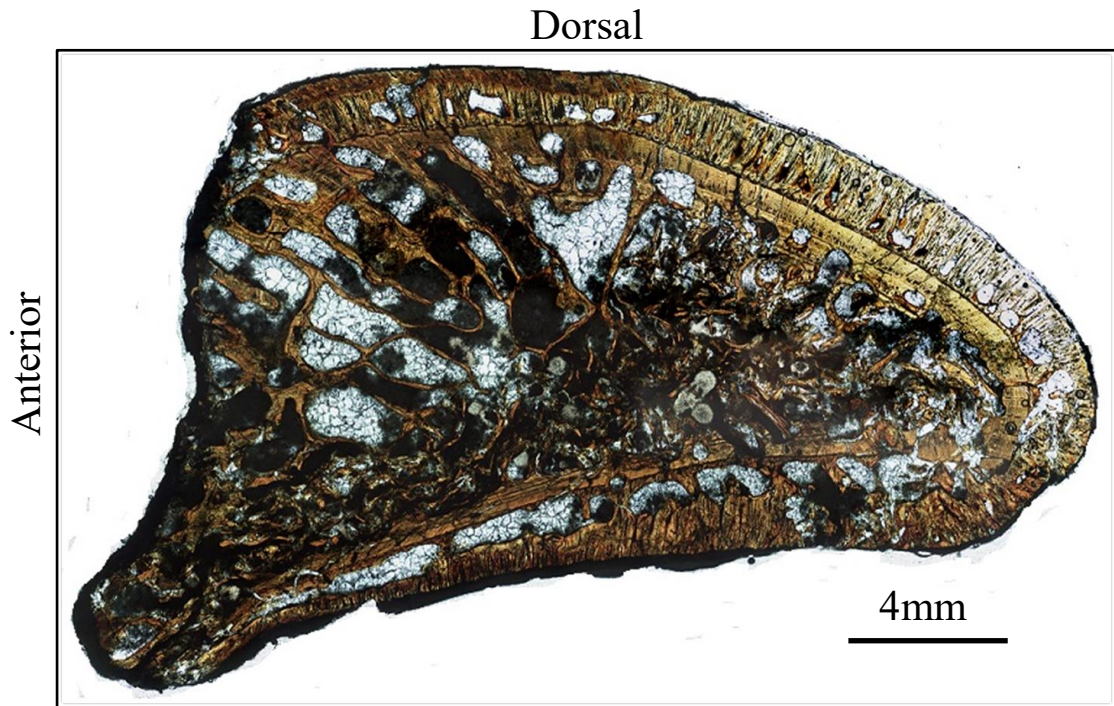


Figure 6: Transverse cross section of ALMNH 5186

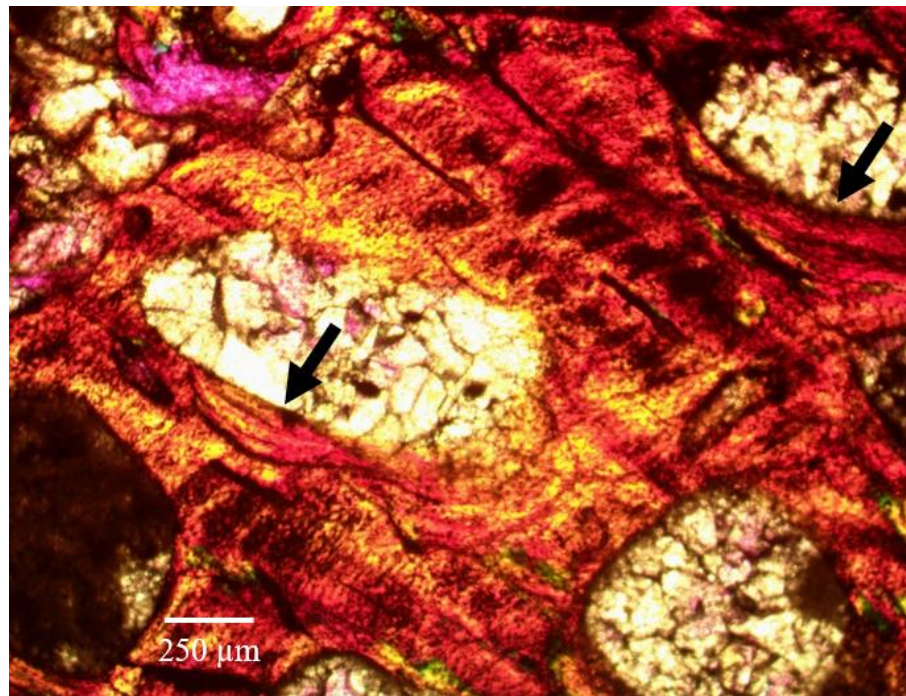


Figure 7: Trabeculae of ALMNH 5186 under polarized light showing reconstruction of bone along edges (black arrows).

Grenzstreifen line marks the change between normal cortical bone and pathological bone (Figure 10); these lines are common when disease or infection cause reactions of abnormal bone growth along the periosteal surface (Rothschild and Martin, 1992 Weston, 2009; Cubo et al., 2015). The osteocyte lacunae are also larger, angular, and more numerous than other areas of the cortical bone (Figure 10). This is another sign of a periosteal reaction caused by infection of disease (Weston, 2009; Redelstorff et al., 2015). Pathologies are common in the mosasaurid fossil record and have been documented on numerous occasions (Rothschild and Martin, 1992; Schulp et al., 2006; Rothschild and Everhart, 2015). No clear cause of the pathology could be seen when examining the humerus and periosteal reactions can stem from a number of causes (Edeikin et al., 1966; Rothschild and Martin, 1992). It is unknown how pathologies affect

Table 3

Measurements (μm) made between the CGMs along Radius B of each humerus. R = resorbed CGMs. Measurements with a * represent the length from the last CGM to the periosteal surface. In RMM 2986, microbial invasion obscured the periosteal surface and most likely obscured 1-2 CGMs

	RMM 6066	ALMNH 5186	ALMNH 4332	RMM 2986
CGM 0-1	-	R	R	R
CGM 1-2	-	632	R	R
CGM 2-3	-	611*	R	R
CGM 3-4	-	-	594	R
CGM 4-5	-	-	646	R
CGM 5-6	-	-	432*	R
CGM 6-7	-	-	-	R
CGM 7-8	-	-	-	274
CGM 8-9	-	-	-	204
CGM 9-10	-	-	-	189
CGM 10-11	-	-	-	211
CGM 11-12	-	-	-	877*
CGM 12-13	-	-	-	

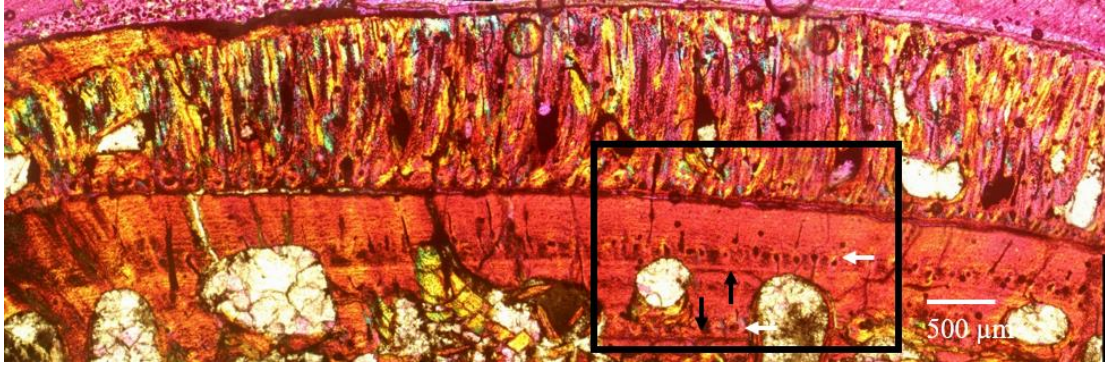


Figure 8: Cortical bone of ALMNH 5186 under polarized light showing two distinct types of bone, rows of longitudinal canals (white arrows), and CGMs (black arrows). Black inset is Figure 9.

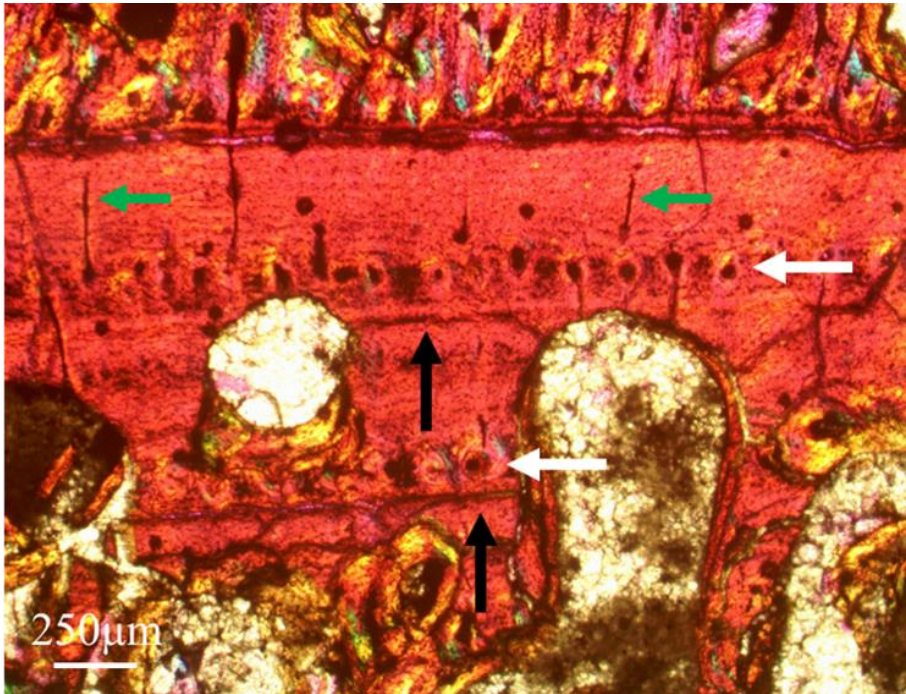


Figure 9: Cortical area of ALMNH 5186 under polarized light with longitudinal canals (white arrows), radial canals (green arrows), and CGMs (black arrows).

the growth of an animal, but the bone already deposited was most likely not impacted – only the bone being laid down at the time of the pathology. Therefore, the cortical area near the endosteum and the medullary region are discussed further. However, because the rate of pathological bone growth is not known, the pathological tissue near the periosteal surface cannot be used to discuss growth rates of this animal. Measurements of the cortical bone did not include the pathological bone. More study of this humerus and bones associated with ALMNH 5186 is needed to understand the pathology, but is out of the scope of this study.

Two CGMs can be seen in the cortical area near the endosteal surface of ALMNH 5186 (Figures 8, 9). These growth marks indicate the animal was at least in its third year at the time of death. Due to minor variation in growth between individuals, the medullary radius of ALMNH 5186 is slightly smaller than the bone radius of RMM 6066. This indicates that CGM #1 in ALMNH 5186 represents the end of the first year of growth and no CGMs were lost due to remodeling. Distance between CGM #1 and CGM #2 in ALMNH 5186 is 632 μm , indicating a growth rate of 1.70 $\mu\text{m}(\text{day})^{-1}$. A third CGM was not laid down. The distance between CGM #2 and the Grenzstreifen line is similar to the distance between CGMs #1 and #2, but it is unknown if the Grenzstreifen line represents a CGM. There is no indication of skeletal maturity at the time of death. The pathological bone found at the periosteum obscures the true periosteal surface and no EFS is seen in or bordering the pathological bone.

Figure 10: Cortical bone of ALMNH 5186 showing the Grenzstreifen line (black arrow) which marks the change from normal cortical bone below the line and pathological cortical bone above the line. Osteocyte lacunae (white arrows) are small and rounded in the normal cortical area and large and angular in the pathological bone.

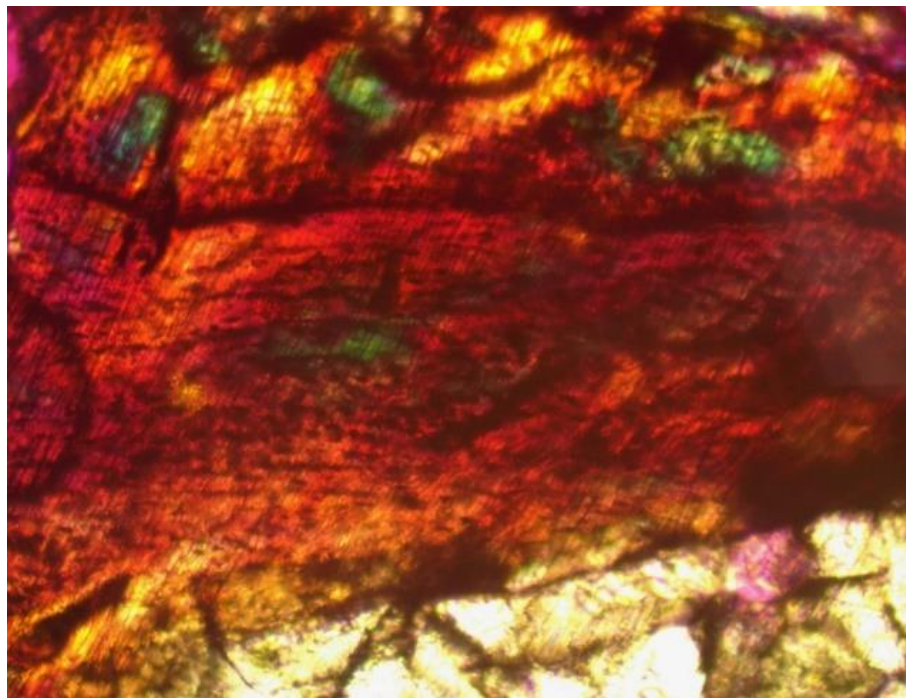
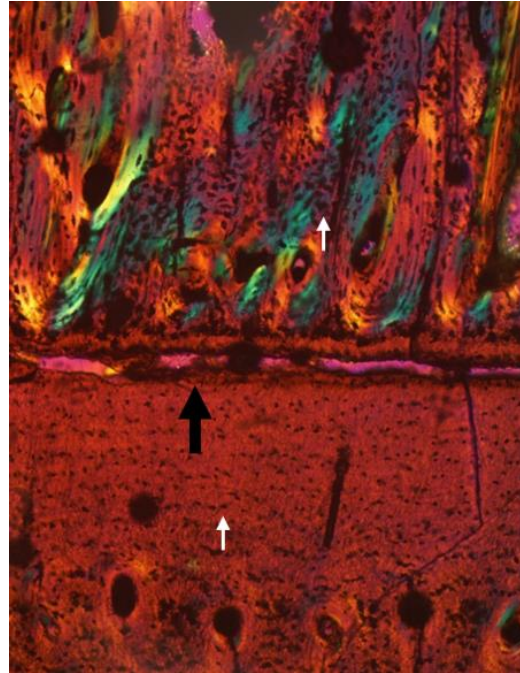


Figure 11: Cortical area of ALMNH 5186 in longitudinal cut under polarized light.

ALMNH 4332

The medullary area of ALMNH 4332 is filled with trabeculae, though many of these trabeculae were crushed after deposition (Figure 12). The trabeculae in the dorsal quadrant are a good indicator of how they appeared before crushing (Figures 12, 13). Most of the trabeculae consist of parallel-fibered bone, though lamellar bone can be seen along the edges (Figure 13). Similar trabecular microstructure was seen in mosasaurid vertebrae by Houssaye and Tafforeau (2012) and in mosasaurid limbs bones by Houssaye et al. (2013). Just as in ALMNH 5186, the cortical bone of ALMNH 4332 appears to be made from woven collagen fibers, but when cut longitudinally, the collagen fibers appear as parallel-fibered bone (Figure 14). Osteocyte lacunae in ALMNH 4332 are small and oblong throughout the trabeculae and cortical bone, in some places appearing almost flat. Longitudinal canals in ALMNH 4332 are not in distinct rows and distances between canals are farther apart than in ALMNH 5186 (Figure 14). The longitudinal vascularity for this bone is $10.41 \text{ canals}(\text{cm}^2)^{-1}$ (Table 2). Longitudinal canals are more numerous near the endosteum with numbers decreasing closer to the periosteum. Near the endosteum, many longitudinal canals have already been expanded by resorption and begun to form the trabecular network.

There are three CGMs observed within the cortical bone of ALMNH 4332 (Figure 15). Retrocalculations indicate two or three CGMs have been lost to resorption (Table 4), making the animal six to seven years old at the time of death. Distances between CGM #1 and CGM #2 are slightly smaller than distances between the next set of CGMs (Table 3) with the highest growth rate of $1.74 \mu\text{m}(\text{day})^{-1}$ represented in the preserved making the

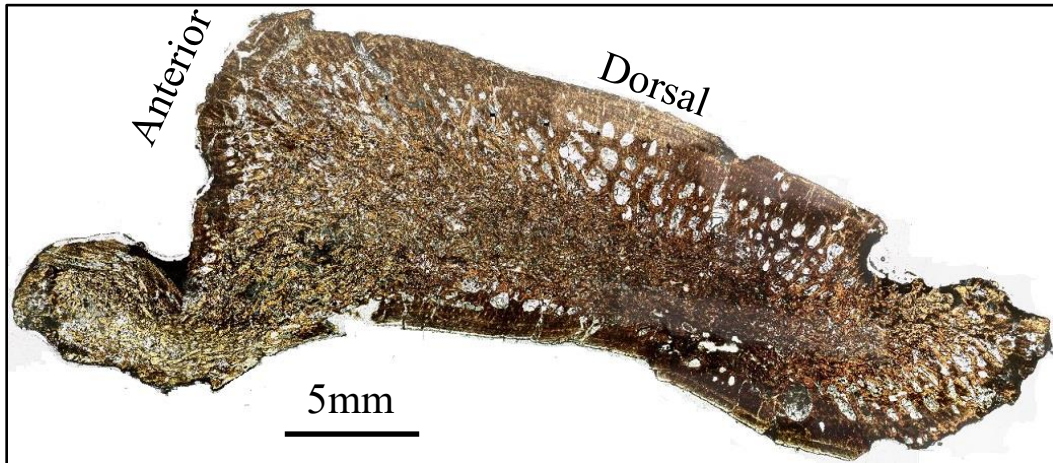


Figure 12: Transverse cross section of ALMNH 4332. Trabeculae in dorsal quadrant represent how trabecular system looked before being crushed taphonomically.

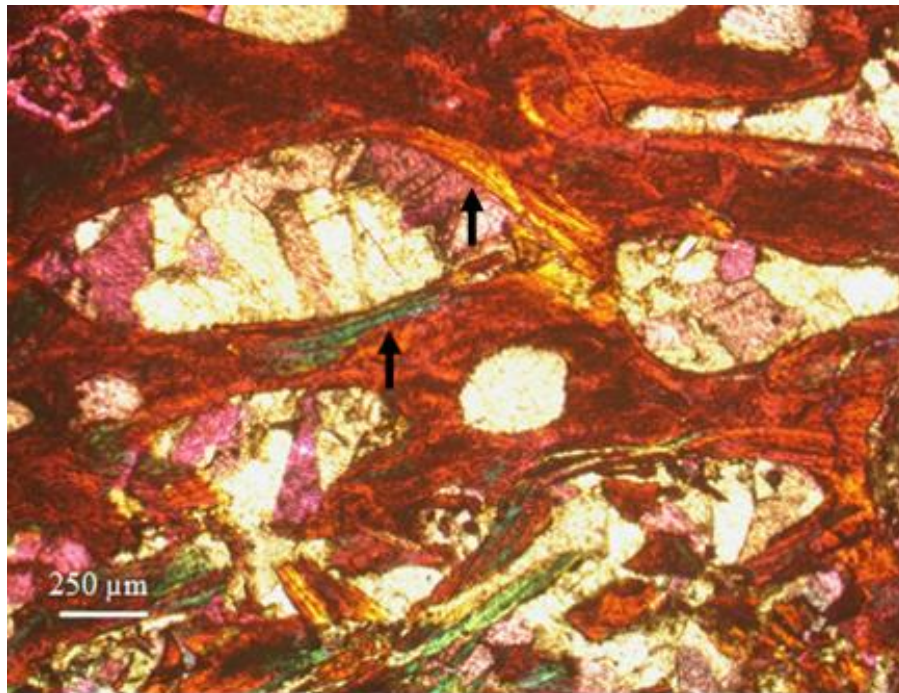


Figure 13: Trabeculae of ALMNH 4332 under polarized light with reconstructed bone along edges (black arrows) and broken trabeculae along the bottom of the photo.

Table 4: Retrocalculations of missing CGMs. All measurements reported in microns. BR, bone radius; CorArea, length of cortical bone from periosteal surface to CGM closest to endosteal surface; MR, medullary radius; RCA, resorbed cortical area; (i), ultimate; (ii), penultimate; (iii), mean; (iv), mean of earlier ontogeny. See Methods for complete details regarding retrocalculations.

Specimen #	BR	CorArea	MR	RCA	# of CGMs	Calculated missing CGMs	Estimated Age
RMM 6066	2840	-	-	-	0		< 1 yr
ALMNH 5186	3920	1240	2680	0	2	0 (i), 0 (ii), 0 (iii), 0 (iv) → 0	3 yrs
ALMNH 4332	5890	1670	4220	1380	3	2-3 (i), 2-3 (ii), 2-3 (iii), 2-3 (iv), → 2-3	6-7 yrs
RMM 2986	7300	1940	5360	2520	5	7-8 (i), 9-10 (ii), 8-9 (iii), 4-5 (iv), → 7-8	13-14 yrs

animal six to seven years old at the time of death. Distances between CGM #1 and CGM #2 are slightly smaller than distances between the next set of CGMs (Table 3) with the highest growth rate of $1.74 \mu\text{m}(\text{day})^{-1}$ represented in the preserved cortical bone of year five (Table 5). The periosteum in ALMNH 4332 is not obscured. There is no evidence of any slowing of growth or an EFS near the periosteum, so this animal was still growing at the time of death.

ALMNH 4332 marks the first appearance of supernumerary growth marks (Figure 15) in the ontogenetic series of this study. Though their significance is unknown, supernumerary growth marks are faint lines that appear between the CGMs and are found in mosasaurids (Pellegrini, 2007), iguanas (Zug and Rand, 1987), and other reptiles (Castanet and Smirina, 1990; Castanet, 1994).

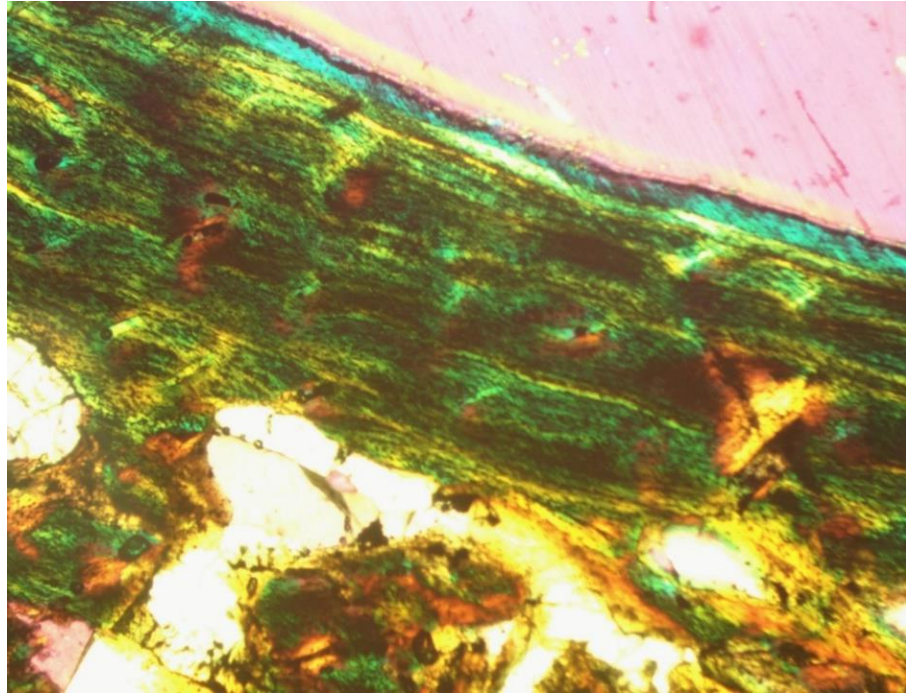


Figure 14: Cortical area of ALMNH 4332 in longitudinal cut under polarized light.

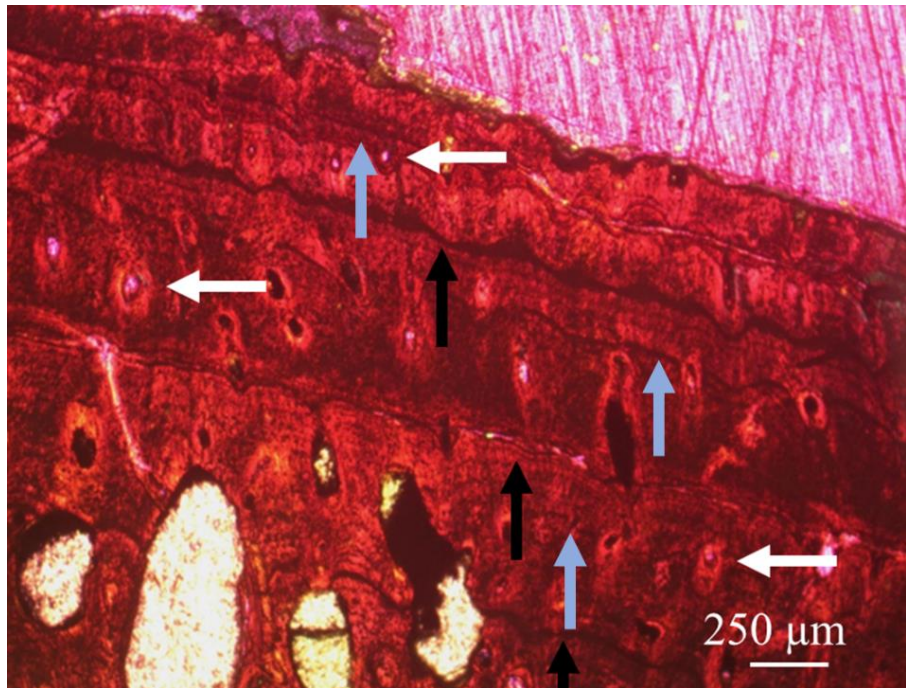


Figure 15: Cortical area of ALMNH 4332 under polarized light with longitudinal vascular canals (white arrows), supernumerary lines (blue arrows), supernumerary lines (black arrows), and CGMs (black arrows).

RMM 2986

The medullary area of RMM 2986 is filled with trabeculae, though many of them were post-depositionally crushed (Figure 16). Uncrushed trabeculae in the dorsal quadrant represent how the medullary area would have appeared (Figures 16, 17). As in ALMNH 4332, the trabeculae consist of parallel-fibered bone, though lamellar bone can be seen along the edges of trabeculae (Figure 17). The cortical bone of RMM 2986 consists of parallel-fibered bone. Osteocyte lacunae are small and rounded and slightly smaller than lacunae seen in previous ontogeny. A row of longitudinally oriented primary osteons and simple canals are situated near the periosteal surface. A row of longitudinally oriented secondary osteons is found just below these primary osteons. Remnants of radial canals are found closer to the endosteum (Figure 18). The overall longitudinal vascularity for this specimen is $1.27 \text{ canals}(\text{cm}^2)^{-1}$ (Table 2).

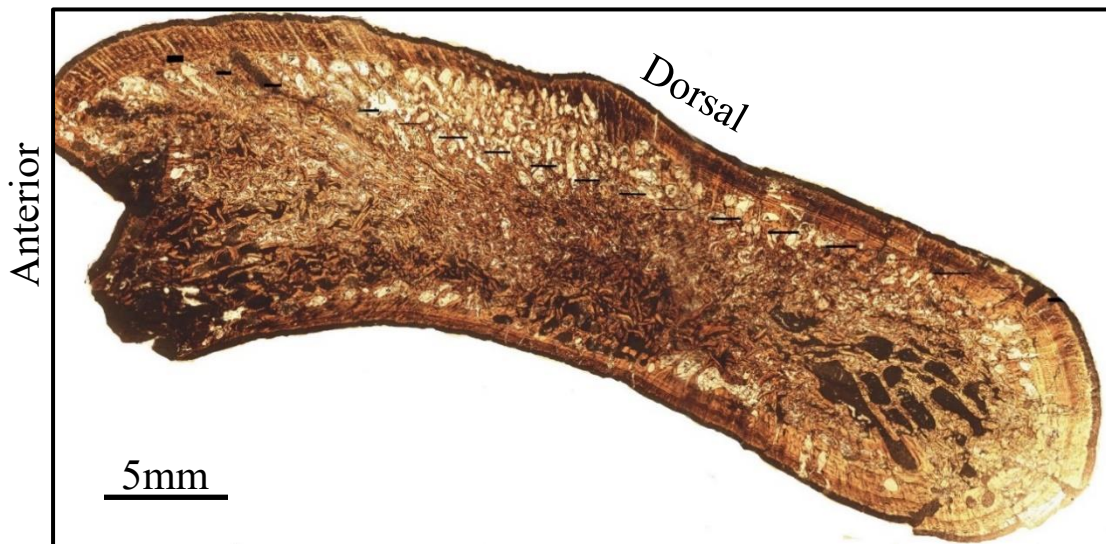


Figure 16: Transverse section of RMM 2986. Medullary area is somewhat crushed though dorsal quadrant has intact trabeculae.

Distinguishing CGMs in RMM 2986 is difficult due to the large number of supernumerary lines (Figure 18), but CGMs are typically darker and thicker than supernumerary marks (Zug and Rand, 1987). Based on this, five CGMs are identified in the cortical bone (Figure 17). Retrocalculations show at least seven or eight CGMs have been resorbed in the medullary area, making the animal 13-14 years of age at the time of death (Table 4). Though distances between CGMs vary from year to year, inter-CGM distances in RMM 2986 are smaller than previous ontogenetic stages studied, with each measurement less than 300 μm (Table 3). The highest growth rate in RMM 2986 is 0.74 $\mu\text{m}(\text{day})^{-1}$ (Table 5). The periosteal surface of RMM 2986 appears dark under polarized light. This is most likely due to postmortem microbial invasion. Because of this contamination, it is unknown if RMM 2986 had an EFS signaling skeletal maturity.

Table 5: Growth rates for each individual per year. Rates were measured by dividing the corresponding CGMs by the days in a Late Cretaceous year (~372) and results are listed in $\mu\text{m}(\text{day})^{-1}$. R = resorbed cortical area. * indicates distance between last CGM and periosteal surface.

	RMM 6066	ALMNH 5186	ALMNH 4332	RMM 2986
Year 1	-	R	R	R
Year 2	-	1.70	R	R
Year 3	-	*	R	R
Year 4	-	-	1.60	R
Year 5	-	-	1.74	R
Year 6	-	-	*	R
Year 7	-	-	-	R
Year 8	-	-	-	0.74
Year 9	-	-	-	0.55
Year 10	-	-	-	0.51
Year 11	-	-	-	0.57
Year 12	-	-	-	*

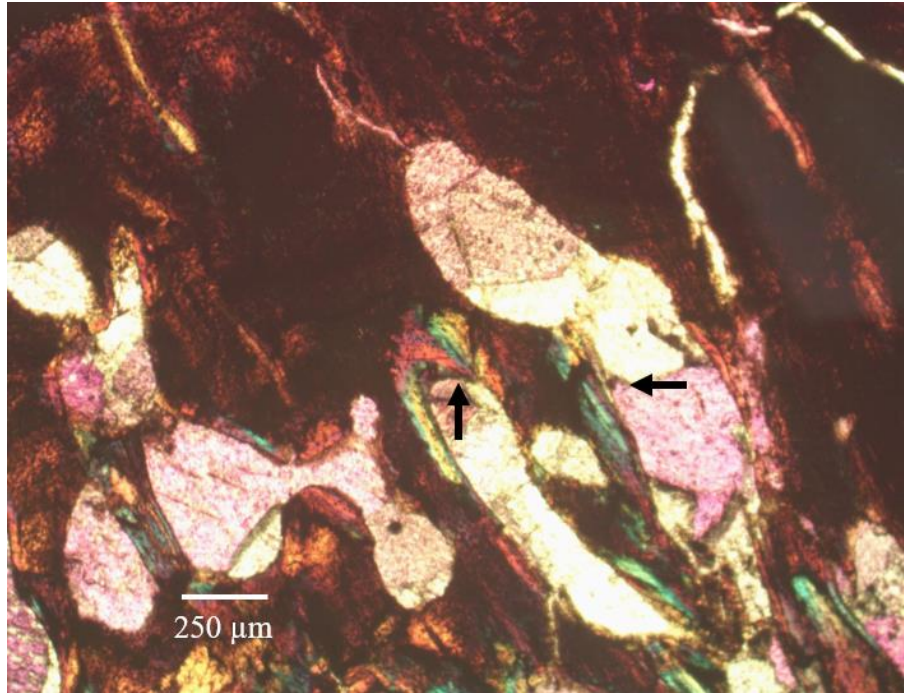


Figure 17: Trabeculae of RMM 2986 under polarized light with areas of reconstructed bone along the edges (black arrows).

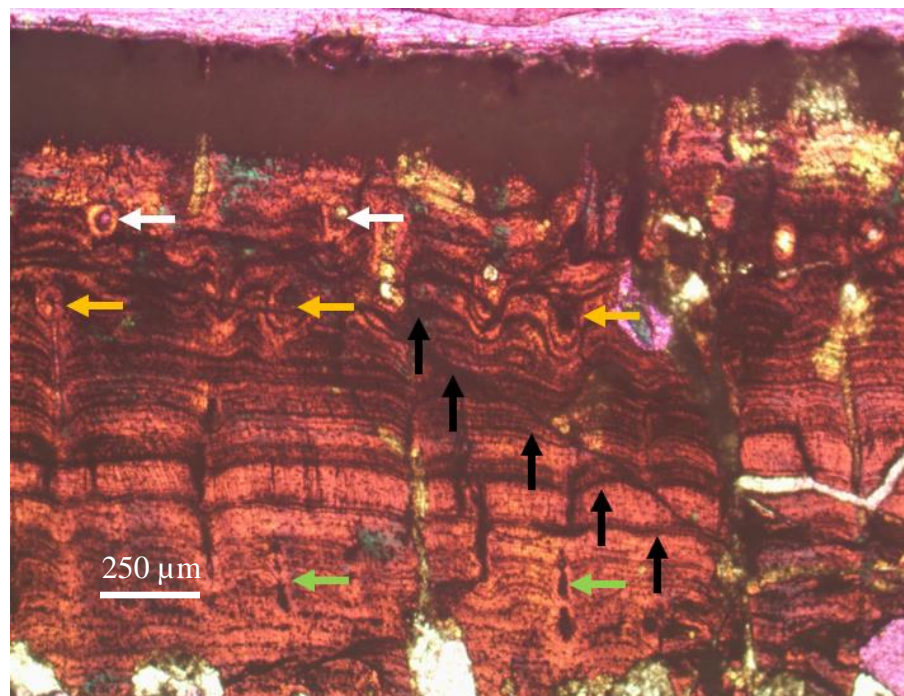


Figure 18: Cortical bone of RMM 2986 under polarized light with longitudinal canals (white arrows), longitudinal secondary canals (yellow arrows), and the remains of some radial canals closer to the endosteal surface. Many supernumerary lines are present between the CGMs (black arrows).

DISCUSSION

The humeri chosen for this study were hypothesized to represent different stages of *Clidastes* ontogeny based on size. Histological testing confirmed that these bones represent yearling, juvenile, sub-adult, and probable adult ontogenetic stages. Each stage is defined by certain characteristics that are unique to that point in ontogeny. No CGMs were reported in the cortical area of RMM 6066 (Figures 4, 5), indicating the animal is in the first year of growth. Radius B of RMM 6066 is close to the medullary radius of ALMNH 5186 (Table 4), indicating RMM 6066 was likely close to the one-year mark when it died. This yearling stage is defined by an open medullary cavity with few trabeculae which do not contain lamellar bone, distinct parallel rows of longitudinally oriented primary osteons, and radial and anastomosing canals open at the periosteum. The juvenile stage is represented by ALMNH 5186 (Figures 1, 6-11). This stage is defined by a partially open medullary area with trabeculae that do contain lamellar bone (indicating new bone construction that strengthens the trabecular walls), longitudinal primary osteons and simple canals arranged in distinct rows, and reconstruction of longitudinal canals into trabecular spaces. The cortical area of the two smallest bones together represent the complete first two and a half years of *Clidastes* ontogeny. The highly vascular nature of a yearling *Clidastes* seen in RMM 6066 has already been lost to resorption in the juvenile ALMNH 5186.

The subadult stage is represented by ALMNH 4332 (Figures 1, 12-15) which was 6 or 7 years old at the time of death (Table 4). This stage is defined by a medullary area filled by trabeculae with lamellar deposits along the edges, scattered simple longitudinal canals, the absence of primary osteons, and supernumerary lines between CGMs. The

largest bone, RMM 2986 (Figures 1, 16-18), represents an individual that was at least 12 to 13 years of age at the time of death (Table 4). Optical clarity is obscured near the periosteal surface due to microbial invasion (Figure 18). This area of microbial invasion measures 877 μm and the previous distance between CGMs was 211 μm so, if growth rates were similar, at least four CGMs are obscured by the microbial invasion; possibly more if growth slowed or stopped. The microbial invasion also prevents assessing this bone for an EFS. Because an EFS denotes skeletal maturity and skeletal maturity is how adulthood is defined (Cormack, 1987; Starck and Chinsamy, 2002; Ponton et al., 2004; Woodward et al., 2011), RMM 2986 cannot be called an adult, but rather is named a probable adult. Because growth rates slow as an animal ages, the slower growth rates seen in RMM 2986 support it being placed in an older ontogenetic stage than other humeri studied (Table 4, 5). This probable adult stage is represented by unorganized longitudinal canals found mostly near the periosteal surface, numerous supernumerary lines between CGMs, and the presence of secondary osteons in the cortical area.

Parallel-fibered bone is the main bone tissue type throughout mosasaurid phylogeny (Houssaye et al., 2013), and this study found parallel-fibered bone tissue throughout *Clidastes* ontogeny. Woven bone was not observed in any bones from this study, and lamellar bone is found only in the trabecular system. Two humeri, ALMNH 5186 and ALMNH 4332, had longitudinally oriented collagen fibers, while the other two had transversely oriented collagen fibers. This explains why the fibers appeared woven in transverse section, but parallel when cut longitudinally. This phenomenon has only been previously noted in archosaurs (Stein and Prondvai, 2014), but this study shows it is also found in squamates.

Besides finding lamellar, parallel-fibered, and woven bone in mosasaurids, Houssaye et al. (2013) added a fourth bone tissue type, unusual parallel-fibered bone (UPFB), described as parallel-fibered bone with larger osteocyte lacunae. Though lacunae were found in parallel-fibered bone in this study, exactly how the size of these lacunae compare to the UPFB lacunae found by Houssaye et al (2013) is unclear due to any definition of lacunae size in Houssaye et al (2013). Size and shape of osteocyte lacunae change through ontogeny in this study, with size of lacunae becoming smaller and shape of lacunae changing from rounded to flattened in later ontogeny.

This study shows that humeral trabeculae are unformed and the medullary area is open during early *Clidastes* ontogeny. As the animal ages, the medullary area is filled with trabeculae. This type of trabecular system is unique among squamates (Houssaye and Bardet, 2012) but is also found in other secondarily aquatic animals unrelated to mosasaurids (de Buffrénil et al., 1990; de Buffrenil and Mazin, 1990; Houssaye, 2013). In the trabecular systems of modern secondarily aquatic mammals (e.g. cetaceans), bone is not fully resorbed along the endosteal surface and deposition takes place at both the periosteal and endosteal surfaces (de Buffrenil, 1988). This seems to be how the trabecular system in mosasaurids is formed as well. The formation of intertrabecular spaces in mosasaurids begins with expansion of primary osteons (Houssaye et al., 2013) and deposition of lamellar bone strengthens the sides of trabeculae (Houssaye and Tafforeau, 2012). This reconstruction process is seen in the trabecular systems of long bones from this study (Figures 7, 13, 17). A fully formed trabecular system is not seen in *Clidastes* ontogeny until the sub-adult stage, represented by ALMNH 4332 (Figure 12).

This is not surprising as the bone of young individuals has not yet had time for the resorption and deposition that constructs the trabeculae to take place.

Houssaye and Tafforeau (2012) show juvenile mosasaurids have a similar vertebral trabecular system as adults. Because medullary compactness in mosasaurid vertebrae is thought to be important for hydrostatic buoyancy and body trim controls (Houssaye and Tafforeau, 2012; Houssaye, 2013), a compact vertebral trabecular system in early ontogeny suggests *Clidastes* were efficient juvenile swimmers (Houssaye and Tafforeau, 2012). In contrast, Bell and Sheldon (1986) show the medullary area in juvenile *Clidastes* ribs is open, while medullary areas of adults are filled with trabeculae. The juvenile *Clidastes* humeri studied herein show a pattern similar to that observed in ribs. Since a juvenile *Clidastes* displays a vertebral medullary area filled with trabeculae but rib and humeral medullary areas that are open, this indicates a different growth pattern between vertebrae and other bones of *Clidastes*. It may be that, because vertebral trabeculae are useful in buoyancy and body trim controls (Houssaye and Tafforeau, 2012), it was beneficial for vertebrae to form trabeculae before ribs or humeri, which are not as important in this function. However, more histological testing on complete specimens is needed to understand the different timing of growth in trabecular systems of *Clidastes*.

Growth Rates

This study shows there is a clear change in vascular density and vascular canal orientation through *Clidastes* ontogeny (Table 2). Vascularization has been shown to correlate with growth rates, with radial and reticular canals considered faster growing than longitudinally oriented canals (de Ricqlès, 1976; de Margerie et al., 2004; de

Buffrenil et al., 2008) and bones with primary osteons growing faster than bones with simple canals (de Margerie et al., 2002). The smallest humerus, RMM 6066, has two times more longitudinal canals(cm^2)⁻¹ than the next smallest bone, and 20 times more than the largest bone. The vascularity of RMM 6066 is made up of radial, reticular, and longitudinal canals, with most longitudinal canals being primary osteons (Figure 5). Exactly how fast RMM 6066 was growing cannot be ascertained because there are no CGMs, but vascularization indicates higher growth in RMM 6066 than other humeri studied. Thus, the fastest growth during *Clidastes* ontogeny occurred during the first year, which is not uncommon among vertebrates (e.g., Horner et al., 2000; Erickson et al., 2004; de Margerie et al., 2004; Cubo et al., 2008).

This high growth rate does not continue after the first year. Longitudinal vascularity decreases in the second smallest bone, ALMNH 5186 (Table 2). The number of reticular and radial canals decreases, and the longitudinal canals are mostly simple canals. This decreasing vascular density represents a slowing of growth. In ALMNH 5186, the distance between CGM #1 and CGM #2 indicates a growth rate of $1.70 \mu\text{m}(\text{day})^{-1}$. This appears to be on the higher end of normal monitor lizard growth (Padian et al., 2001; Montes et al., 2007; Cubo et al., 2008). While it is unknown how fast RMM 6066 was growing during that first year, vascularity indicates it was growing faster than the $1.70 \mu\text{m}(\text{day})^{-1}$ found in ALMNH 5186. Cubo et al. (2012) documented some newborn monitor lizards growing upwards of $7\text{-}9 \mu\text{m}(\text{day})^{-1}$ but whether the yearling *Clidastes* could reach that level is unknown.

Overall vascularity and growth rate in the second largest bone, ALMNH 4332, is similar to that seen in ALMNH 5186 (Table 2 and 3). The distances between CGM #1

and CGM #2 in ALMNH 4332 indicate a growth rate of $1.60 \mu\text{m}(\text{day})^{-1}$ (Table 3). This is only slightly smaller than in ALMNH 5186. The distance between CGM #2 and CGM #3 in ALMNH 4332 indicates a growth rate of $1.74 \mu\text{m}(\text{day})^{-1}$ (Table 3). The variance between CGMs is probably due to individual variability in skeletal growth possibly attributed to nutrition and water quality (Stamps and Tanaka, 1981; de Buffrenil and Castanet, 2000). The slight change in average growth rate between ALMNH 5186 and ALMNH 4332 most likely represents individual variation rather than ontogenetic changes in growth. This indicates that after a sharp decrease in rates during year one, growth in *Clidastes* remained relatively constant between at least the second and seventh year.

RMM 2986 has the lowest vascularity of any bone studied (Table 2), indicating an animal with much slower growth rates. The distances between CGMs in RMM 2986 also decrease substantially (Table 3), resulting in lower absolute bone apposition rates as well (Table 5). The differences in vascularity, distances between GCMs, and growth rates between RMM 2986 and smaller humeri are substantial enough to be considered a true slowing of growth rather than just individual variation (Table 3, 5). Accounting for retrocalculations, the slowing of growth observed between the late-sub adult and adult stage represented by RMM 2986 occurs between the ages of seven and nine (Tables 4, 5). A slowing of growth prior to skeletal maturity has been shown to occur when sexual maturity is reached in extant animals (Brody, 1964; Reiss, 1989; Lee and Werning, 2008). Based on growth curves derived from histological testing, Pellegrini (2007) concluded that a slowing of growth in mosasaurids happened when sexual maturity was reached between ages five and seven, the same age sexual maturity is reached in modern, large varanids (i.e. the Komodo Dragon). Evidence presented here shows that *Clidastes*

growth remains constant until at least age seven. If a decrease in growth rate does signal sexual maturity in *Clidastes* (*sensu* Pellegrini, 2007), the results of this study indicates sexual maturity was reached around year seven or eight in *Clidastes*.

Clidastes metabolism

Ectothermic animals have slower growth rates than endothermic animals (Padian et al., 2001; Sander and Andrassy, 2006; Montes et al., 2007; Cubo et al., 2012; Köhler et al., 2012). Harrell et al. (2016) determined an endothermic metabolism for *Clidastes* because body temperatures were above the ambient sea temperatures and closer to the temperatures found in endothermic pelagic sea birds. However, if *Clidastes* was endothermic, growth rates indicating an endothermic metabolism are expected. The results of this study do not support an endothermic metabolism for *Clidastes*. No growth rates calculated here approach modern endotherms, which have growth rates higher than $15+ \mu\text{m}(\text{day})^{-1}$ (Padian et al., 2001; de Margerie et al., 2004). Rather, this study found rates closer to ectothermic varanids such as the monitor lizard, indicating an ectothermic metabolism. It is important to note that these results do not imply that the temperatures derived from isotopic studies are incorrect. A gigantothermic metabolism would have allowed large *Clidastes* to hold higher body temperatures but still have growth rates comparable to an ectothermic metabolism. The specimens used in Harrell et al. (2016) were large jaws, which most likely belonged to specimens in late ontogeny. The large size of these specimens could enable them to maintain gigantothermy. This gigantothermic hypothesis could be tested by analyzing isotopes from teeth of smaller *Clidastes* representing ontogenetically younger specimens. According to the findings from this study, isotopic analysis of the smaller individuals would most likely show lower

metabolic temperatures than those found in the Harrell et al. (2016) study and indicate that *Clidastes* was gigantothermic late in ontogeny when larger sizes were reached.

CONCLUSION

This study came to three main conclusions regarding *Clidastes* ontogenetic growth. First, as body size and age increase in *Clidastes*, vascularity and growth rates decrease. *Clidastes* yearlings (RMM 6066) were equipped with well vascularized bone tissue that allowed them to grow quickly during their first year. After the first year, growth slowed considerably, falling to below half of the first-year rate. The growth rate of a juvenile (ALMNH 5186) is marked by this decline in vascularity and loss of primary osteons and anastomosing canals. Vascularity and growth rate remain do not change in the sub-adult (ALMNH 4332), remaining similar to the juvenile, but longitudinal canals arranged less linearly can differentiate the sub-adult stage. After the age of seven or eight, growth in *Clidastes* slowed again and the slower rates seen in the probable adult (RMM 2986) were reached. Unfortunately, skeletal maturity could not be determined due to microbial invasion in the bones of the oldest *Clidastes* specimen.

Second, the medullary area of *Clidastes* humeri remains partially open through the first few years of life, becoming more compact as the animal reaches sub-adulthood. After sub-adulthood, the medullary area became filled with trabeculae as cortical bone is continually resorbed and reconstructed into trabeculae and longitudinal canals were widened to form the trabecular spaces.

Third, growth rates in *Clidastes* are more similar to modern animals with ectothermic rather than endothermic metabolisms. Previous work described *Clidastes* growth as faster than monitor lizards based on *Clidastes* having a higher vascular density (Houssaye and Tafforeau, 2012; Houssaye et al., 2013). Though this study did find that *Clidastes* had a higher vascular density than monitor lizards, bone growth in microns per

day was similar to growth in monitor lizards with growth rates from all specimens below $2.0 \mu\text{m}(\text{day})^{-1}$. The yearling (RMM 6066) most likely had slightly elevated growth rates than the ontogenetically older individuals, but this elevated rate was only seen the first year. Consequently, this study did not find that *Clidastes* had growth rates similar to modern endothermic animals. Rather, the growth rates calculated in this study show *Clidastes* growth more in line with ectothermic varanids. This study could find no evidence of endothermy in *Clidastes* and considers them either ectothermic animals like modern varanids or gigantothermic animals like some modern sea turtles.

LITERATURE CITED

- Amprino, R. 1947. La structure du tissu osseux envisagée comme expression de différences dans la vitesse de l'accroissement. *Archives de Biologie* 58:317–330.
- Bell, G. L. 1997. A phylogenetic revision of North American and Adriatic Mosasuroidea; pp. 293–332 in Callaway, J.M. and E.L. Nichols (eds.), *Ancient Marine Reptiles*. Academic Press, San Diego, CA, USA.
- Bell, G. L., and M. A. Sheldon. 1986. Description of a very young mosasaur, Alabama. *Journal of the Alabama Academy of Sciences* 57:76–82.
- Bernard, A., C. Lecuyer, P. Vincent, R. Amiot, N. Bardet, E. Buffetaut, G. Cuny, F. Fourel, F. Martineau, J.-M. Mazin, and A. Prieur. 2010. Regulation of body temperature by some Mesozoic marine reptiles. *Science* 328:1379–1382.
- Brody, S. 1964. *Bioenergetics and Growth: With Special Reference to the Efficiency Complex in Domestic Animals*, 2nd ed. Hafner, New York, USA.
- de Buffrenil, V. 1988. On how the periosteal bone of the delphinid humerus becomes cancellous: Ontogeny of a histological specialization. *Journal of Morphology* 198:149–164.
- de Buffrenil, V., and J.-M. Mazin. 1990. Bone histology of the ichthyosaurs: comparative data and functional interpretation. *Paleobiology* 16:435–447.
- de Buffrenil, V., and J. Castanet. 2000. Age estimation by skeletochronology in the Nile monitor (*Varanus niloticus*), a highly exploited species. *Journal of Herpetology* 34:414.
- de Buffrenil, V., A. Houssaye, and W. Bohme. 2008. Bone vascular supply in monitor lizards (Squamata: Varanidae): Influence of Size, Growth, and Phylogeny. *Journal of Morphology* 269:533–543.
- de Buffrenil, V., A. de Ricqlès, C. E. Ray, and D. P. Domning. 1990. Bone histology of the ribs of the archaeocetes (Mammalia: Cetacea). *Journal of Vertebrate Paleontology* 10:455–466.
- Caldwell, M. W. 2002. From fins to limbs to fins: Limb evolution in fossil marine reptiles. *American Journal of Medical Genetics* 112:236–249.
- Caldwell, M. W., and M. S. Y. Lee. 2001. Live birth in Cretaceous marine lizards (mosasauroids). *Proceedings of the Royal Society B: Biological Sciences* 268:2397–2401.
- Castanet, J. 1994. Age estimation and longevity in reptiles. *Gerontology* 40:174–192.
- Castanet, J., and E. Smirina. 1990. Introduction to the skeletochronological method in amphibians and reptiles. *Annales de Sciences Naturelles, Zoologie* 11:191–196.
- Castanet, J., K. C. Rogers, J. Cubo, and J. Jacques-Boisard. 2000. Periosteal bone growth rates in extant ratites (ostrich and emu). Implications for assessing growth in dinosaurs. *Comptes Rendus de l'Académie Des Sciences-Series III-Sciences de La Vie* 323:543–550.
- Chinsamy, A. 1993. Bone histology and growth trajectory of the prosauropod dinosaur *Massospondylus carinatis* Owen. *Modern Geology* 18:319–329.
- Chinsamy, A. 1995. Ontogenetic changes in the bone histology of the Late Jurassic ornithomimid *Dryosaurus lettowvorbecki*. *Journal of Vertebrate Paleontology* 15:96–104.

- Chinsamy, A., and J. H. Hurum. 2006. Bone microstructure and growth patterns of early mammals. *Acta Palaeontologica Polonica* 51:325–338.
- Conrad, J. L., O. Rieppel, and L. Grande. 2008. Re-assessment of varanid evolution based on new data from *Saniwa ensidens* Leidy, 1870 (Squamata, Reptilia). *American Museum Novitates* 1–15.
- Cormack, D. H. 1987. *Ham's Histology*. Lippincott Williams & Wilkins, Philadelphia, PA, 732 pp.
- Cubo, J., N. Le Roy, C. Martinez-Maza, and L. Montes. 2012. Paleohistological estimation of bone growth rate in extinct archosaurs. *Paleobiology* 38:335–349.
- Cubo, J., H. Woodward, E. Wolff, and J. R. Horner. 2015. First reported cases of biomechanically adaptive bone modeling in non-avian dinosaurs. *PloS One* 10:e0131131.
- Cubo, J., P. Legendre, A. De Ricqlès, L. Montes, E. De Margerie, J. Castanet, and Y. Desdevises. 2008. Phylogenetic, functional, and structural components of variation in bone growth rate of amniotes. *Evolution & Development* 10:217–227.
- Curry, K. A. 1999. Ontogenetic histology of *Apatosaurus* (Dinosauria: Sauropoda): New insights on growth rates and longevity. *Journal of Vertebrate Paleontology* 19:654–665.
- Edeikin, J., P. J. Hodes, and L. Caplan. 1966. New bone production and periosteal reaction. *American Journal of Roentgenology* 97:708–718.
- Erickson, G. 2000. Growth curve of *Psittacosaurus mongoliensis* Osborn (Ceratopsia: Psittacosauridae) inferred from long bone histology. *Zoological Journal of the Linnean Society* 130:551–566.
- Erickson, G. M., P. J. Makovicky, P. J. Currie, M. A. Norell, S. A. Yerby, and C. A. Brochu. 2004. Gigantism and comparative life-history parameters of tyrannosaurid dinosaurs. *Nature* 430:772–775.
- Field, D. J., A. LeBlanc, A. Gau, and A. D. Behlke. 2015. Pelagic neonatal fossils support viviparity and precocial life history of Cretaceous mosasaurs. *Palaeontology* 58:401–407.
- Harrell, T. L., A. Pérez-Huerta, and C. A. Suarez. 2016. Endothermic mosasaurs? Possible thermoregulation of Late Cretaceous mosasaurs (Reptilia, Squamata) indicated by stable oxygen isotopes in fossil bioapatite in comparison with coeval marine fish and pelagic seabirds. *Palaeontology* 59.3:351–363.
- Horner, J. R., and K. Padian. 2004. Age and growth dynamics of *Tyrannosaurus rex*. *Proceedings of the Royal Society B: Biological Sciences* 271:1875–1880.
- Horner, J. R., A. De Ricqlès, and K. Padian. 2000. Long bone histology of the hadrosaurid dinosaur *Maiasaura peeblesorum*: Growth dynamics and physiology based on an ontogenetic series of skeletal elements. *Journal of Vertebrate Paleontology* 20:115–129.
- Houssaye, A. 2008. A preliminary report on the evolution of the vertebral microanatomy within mosasauroids (Reptilia, Squamata). *Proceedings of the Second Mosasaur Meeting* 81–89.
- Houssaye, A. 2009. “Pachyostosis” in aquatic amniotes: A review. *Integrative Zoology* 4:325–340.

- Houssaye, A. 2013. Bone histology of aquatic reptiles: What does it tell us about secondary adaptation to an aquatic life? *Biological Journal of the Linnean Society* 108:3–21.
- Houssaye, A., and N. Bardet. 2012. Rib and vertebral micro-anatomical characteristics of hydropelvic mosasauroids. *Lethaia* 45:200–209.
- Houssaye, A., and P. Tafforeau. 2012. What vertebral microanatomy reveals about the ecology of juvenile mosasaurs (Reptilia, Squamata). *Journal of Vertebrate Paleontology* 32:1042–1048.
- Houssaye, A., P. Tafforeau, C. de Muizon, and P. D. Gingerich. 2015. Transition of Eocene whales from land to sea: Evidence from bone microstructure. *PLOS ONE* 10:e0118409.
- Houssaye, A., J. Lindgren, R. Pellegrini, A. H. Lee, D. Germain, and M. J. Polcyn. 2013. Microanatomical and histological features in the long bones of mosasaurine mosasaurs (Reptilia, Squamata) – Implications for aquatic adaptation and growth rates. *PLoS ONE* 8:e76741.
- Kiernan, C. R. 2002. Stratigraphic distribution and habitat segregation of mosasaurs in the Upper Cretaceous of western and central Alabama, with an historical review of Alabama mosasaur discoveries. *Journal of Vertebrate Paleontology* 22:91–103.
- King, D., and B. Green. 1999. *Goannas: The Biology of Varanid Lizards*. UNSW Press, 116 pp.
- Köhler, M., N. Marín-Moratalla, X. Jordana, and R. Aanes. 2012. Seasonal bone growth and physiology in endotherms shed light on dinosaur physiology. *Nature* 487:358–361.
- Lamm, E.-T. 2013. Preparation and Sectioning of Specimens; pp. 64–157 in K. Padian and E.-T. Lamm (eds.), *The Bone Histology of Fossil Tetrapods*. University of California Press, Los Angeles, CA, USA.
- Lee, A. H., and S. Werning. 2008. Sexual maturity in growing dinosaurs does not fit reptilian growth models. *Proceedings of the National Academy of Sciences* 105:582–587.
- Lee, A. H., A. K. Huttenlocker, K. Padian, and H. N. Woodward. 2013. Analysis of growth rates; pp. 217–252 in K. Padian and E.-T. Lamm (eds.), *Bone Histology of Fossil Tetrapods: Advancing Methods, Analysis, and Interpretation*. University of California Press, Los Angeles, CA.
- Lee, M. S. 1997. The phylogeny of varanoid lizards and the affinities of snakes. *Philosophical Transactions of the Royal Society of London B: Biological Sciences* 352:53–91.
- Lindgren, J., M. J. Polcyn, and B. A. Young. 2011. Landlubbers to leviathans: Evolution of swimming in mosasaurine mosasaurs. *Paleobiology* 37:445–469.
- Liu, K. 2009. Oxygen and carbon isotope analysis of the Mooreville Chalk and late Santonian-early Campanian sea level and sea surface temperature changes, northeastern Gulf of Mexico, U.S.A. *Cretaceous Research* 30:980–990.
- de Margerie, E., J. Cubo, and J. Castanet. 2002. Bone typology and growth rate: testing and quantifying “Amprino's rule” in the mallard (*Anas platyrhynchos*). *Comptes Rendus Biologies* 325:221–230.
- de Margerie, E., J.-P. Robin, D. Verrier, J. Cubo, R. Groscolas, and J. Castanet. 2004. Assessing a relationship between bone microstructure and growth rate: A

- fluorescent labelling study in the king penguin chick (*Aptenodytes patagonicus*). *Journal of Experimental Biology* 207:869–879.
- Montes, L., N. Le Roy, M. Perret, V. De Buffrenil, J. Castanet, and J. Cubo. 2007. Relationships between bone growth rate, body mass and resting metabolic rate in growing amniotes: A phylogenetic approach. *Biological Journal of the Linnean Society* 92:63–76.
- Padian, K., and K. Stein. 2013. Evolution of Growth Rates; pp. 253–264 in K. Padian and E.-T. Lamm (eds.), *Bone Histology of Fossil Tetrapods: Advancing Methods, Analysis, and Interpretation*. University of California Press, Los Angeles, CA.
- Padian, K., A. J. de Ricqlès, and J. R. Horner. 2001. Dinosaurian growth rates and bird origins. *Nature* 412:405–408.
- Padian, K., J. R. Horner, and A. De Ricqlès. 2004. Growth in small dinosaurs and pterosaurs: the evolution of archosaurian growth strategies. *Journal of Vertebrate Paleontology* 24:555–571.
- Paladino, F. V., M. P. O'Connor, and J. R. Spotila. 1990. Metabolism of leatherback turtles, gigantothermy, and thermoregulation of dinosaurs. *Nature* 344:858.
- Pellegrini, R. 2007. Skeletochronology of the limb elements of mosasaurs (Squamata; Mosasauridae). *Transactions of the Kansas Academy of Science* 110:83–99.
- Ponton, F., A. Elżanowski, J. Castanet, A. Chinsamy, E. D. Margerie, A. D. Ricqlès, and J. Cubo. 2004. Variation of the Outer Circumferential Layer in the Limb Bones of Birds. *Acta Ornithologica* 39:137–140.
- Redelstorff, R., S. Hayashi, B. M. Rothschild, and A. Chinsamy. 2015. Non-traumatic bone infection in stegosaurs from Como Bluff, Wyoming. *Lethaia* 48:47–55.
- Reiss, M. J. 1989. *The Allometry of Growth and Reproduction*. Cambridge University Press, New York, 200 pp.
- de Ricqlès, A. 1976. On bone histology of fossil and living reptiles, with comments on its functional and evolutionary significance. *Morphology and Biology of Reptiles* 3:123–149.
- Rothschild, B., and M. J. Everhart. 2015. Co-ossification of vertebrae in mosasaurs (Squamata, Mosasauridae); evidence of habitat interactions and susceptibility to bone disease. *Transactions of the Kansas Academy of Science* 118:265–275.
- Rothschild, B. M., and L. D. Martin. 1992. *Paleopathology: Disease in the Fossil Record*. CRC Press, Boca Raton, FL. 386 pp.
- Sander, D. P. M., and P. Andrassy. 2006. Lines of arrested growth and long bone histology in Pleistocene large mammals from Germany: What do they tell us about dinosaur physiology? *Palaeontographica Abteilung A* 277:143–159.
- Sander, P. M., and C. Tückmantel. 2003. Bone lamina thickness, bone apposition rates, and age estimates in sauropod humeri and femora. *Paläontologische Zeitschrift* 77:161–172.
- Schulp, A. S., G. Walenkamp, P. A. Hofman, Y. Stuij, and B. M. Rothschild. 2006. Chronic bone infection in the jaw of *Mosasaurus hoffmanni* (Squamata). *Oryctos* 6:41–52.
- Sheldon, A. 1997. Ecological implications of mosasaur bone microstructure; pp. 333–351 in Callaway, J.M. and E.L. Nichols (eds.), *Ancient Marine Reptiles*. Academic Press, San Diego, CA, USA.

- Stamps, J., and S. Tanaka. 1981. The influence of food and water on growth rates in a tropical lizard (*Anolis aeneus*). *Ecology* 62:33–40.
- Starck, J. M., and A. Chinsamy. 2002. Bone microstructure and developmental plasticity in birds and other dinosaurs. *Journal of Morphology* 254.3:232–246.
- Stein, K., and E. Prondvai. 2014. Rethinking the nature of fibrolamellar bone: an integrative biological revision of sauropod plexiform bone formation. *Biological Reviews* 89:24–47.
- Wells, J. W. 1969. Coral growth and geochronometry. *Nature* 197:948–950.
- Weston, D. A. 2009. Paleohistopathological analysis of pathology museum specimens: Can periosteal reaction microstructure explain lesion etiology? *American Journal of Physical Anthropology* 140:186–193.
- Woodward, H., K. Padian, and A. H. Lee. 2013. Skeletochronology; pp. 195–215 in K. Padian and E.-T. Lamm (eds.), *Bone Histology of Fossil Tetrapods: Advancing Methods, Analysis, and Interpretation*. University of California Press, Los Angeles, CA.
- Woodward, H. N., J. R. Horner, and J. O. Farlow. 2011. Osteohistological evidence for determinate growth in the American alligator. *Journal of Herpetology* 45:339–342.
- Woodward, H. N., J. R. Horner, and J. O. Farlow. 2014. Quantification of intraskeletal histovariability in *Alligator mississippiensis* and implications for vertebrate osteohistology. *PeerJ* 2:e422.
- Zug, G. R., and A. S. Rand. 1987. Estimation of age in nesting female *Iguana iguana*: Testing skeletochronology in a tropical lizard. *Amphibia-Reptilia* 8:237–249.

**Fort Hays State University
FHSU Scholars Repository
Non-Exclusive License Author Agreement**

I hereby grant Fort Hays State University an irrevocable, non-exclusive, perpetual license to include my thesis ("the Thesis") in *FHSU Scholars Repository*, FHSU's institutional repository ("the Repository").

I hold the copyright to this document and agree to permit this document to be posted in the Repository, and made available to the public in any format in perpetuity.

I warrant that the posting of the Thesis does not infringe any copyright, nor violate any proprietary rights, nor contains any libelous matter, nor invade the privacy of any person or third party, nor otherwise violate FHSU Scholars Repository policies.

I agree that Fort Hays State University may translate the Thesis to any medium or format for the purpose of preservation and access. In addition, I agree that Fort Hays State University may keep more than one copy of the Thesis for purposes of security, back-up, and preservation.

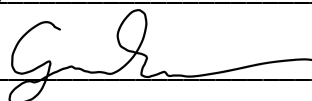
I agree that authorized readers of the Thesis have the right to use the Thesis for non-commercial, academic purposes, as defined by the "fair use" doctrine of U.S. copyright law, so long as all attributions and copyright statements are retained.

To the fullest extent permitted by law, both during and after the term of this Agreement, I agree to indemnify, defend, and hold harmless Fort Hays State University and its directors, officers, faculty, employees, affiliates, and agents, past or present, against all losses, claims, demands, actions, causes of action, suits, liabilities, damages, expenses, fees and costs (including but not limited to reasonable attorney's fees) arising out of or relating to any actual or alleged misrepresentation or breach of any warranty contained in this Agreement, or any infringement of the Thesis on any third party's patent, trademark, copyright or trade secret.

I understand that once deposited in the Repository, the Thesis may not be removed.

Thesis: OSTEOHISTOLOGY AND SKELETOCHRONOLOGY OF AN ONTOGENETIC
SERIES OF CLIDASTES (SQUAMATA: MOSASAURIDAE): GROWTH
AND METABOLISM IN BASAL MOSASAURIDS

Author: Cyrus C. Green

Signature: 

Date: 12/21/2018